Accurate Simulation of Voltage Amplification in High-Performance MEMS-based Matching Networks

Luca Colombo*, Giuseppe Michetti*, Pietro Simeoni*, Mary E. Galanko Klemash†,
Tobias M. Kiebala‡, Sarah S. Bedair†, and Matteo Rinaldi*
*SMART Center, Northeastern University, Boston MA, USA
†U.S. Army Combat Capabilities Development Command - Army Research Laboratory, Adelphi MD, USA
‡Rochester Institute of Technology, Rochester NY, USA

***Abstract*—This paper investigates different methods to estimate the passive voltage amplification (or gain, G_v) provided by high-performance microelectromechanical acoustic systems (MEMS) matching networks in novel Internet of Things wake-up architectures. A brief modeling of the devices and of G_v is provided. Three different methods, leveraging both measured and extrapolated data, are presented. As a case study, measurements of a fabricated X-cut S_0 mode Lithium Niobate (LN) resonator operating around 200 MHz are reported and discussed, with a specific focus on parasitics modeling. Electromagnetic (EM) simulations are used in this framework to provide a robust approach to substrate losses and non-idealities. Simulations of G_v are compared with direct measurement of passive voltage amplification performed on the LN resonator (G_v = 29 dB at 203 MHz for a C_{load} of 270 fF), ultimately confirming that the best gain estimation method is given by combining multimode device fitting and EM simulations for substrate losses characterization.**

***Index Terms*—MEMS; RF passive voltage gain; WuRx; IoT**

I. Introduction

EVENT-driven, ultra low power unattended sensors have been gathering research interest in recent years for distributed wireless networks such as Internet of Things (IoT) applications [1] [2] [3]. In this context, novel asynchronous receivers (Rx) architectures capable to detect signals as low as -100 dBm with ultra-low power consumption down to tens of nW have been demonstrated [4] [5], breaking a power-sensitivity paradigm that has been in place for decades, and paving the way for the development of perpetual, real-time monitoring remote sensors.

In order to break this paradigm, these applications require the complete re-design of the radio frequency front-end (RFFE). The desired RFFE features include high passive voltage amplification to ease baseband (BB) CMOS operations, and aggressive filtering for interference suppression and enhanced false alarm error rate [6], which directly translate into the need for high quality factor (Q) passive components. For this reason, matching networks (MN) implemented via piezoelectric resonators have been proposed for this environment [7]. Recently, G_v greater than 30 dB and bandwidth (BW_{3dB}) of tens of kHz have been demonstrated in the sub-GHz range [8]. These results are enabled by recent advancements in microelectromechanical systems (MEMS) materials, processing, and design [9] [10] [11], allowing to outperform the performance achievable with commercially available components by one order of magnitude [8].

To this end, the direct measurement of the passive voltage provided by MEMS resonators used as MN (Fig. 1a) suffers from practical challenges : G_v is load-dependent, and given the high-Q, high-impedances in play, conventional measurements performed on 50 Ω Vector Network Analyzers are not suitable for the task. Therefore, expensive specialized instrumentation is required.

Furthermore, conventional simulation techniques based on direct measurements are limited by the noise floor and the dynamic range of the measurement instruments. In this paper, different methods for the accurate simulation of passive voltage amplification in MEMS-based matching networks are investigated. In the first section, the resonator and different gain models are introduced. In the second part, simulations and measurements are reported. In the third and last section, results are discussed.

II. Modeling

A. RFFE and Acoustic Resonator

A simple electrical model describing a RFFE including a resonator-based matching network is reported in Fig.1b. In this configuration, the resonator interfaces the antenna (R_{in} = 50 Ω) to the capacitive input stage of an envelope detector (C_{load}).

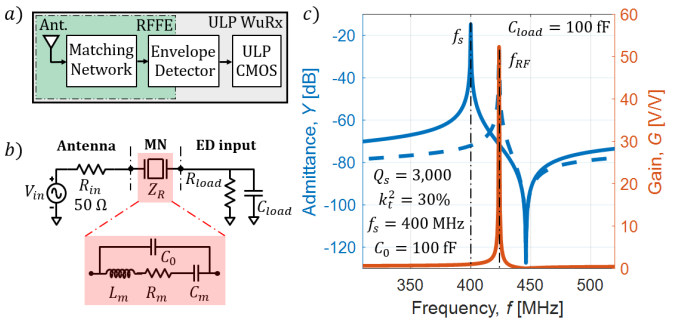

Fig. 1. a) Generic schematic of a novel, asynchronous Ultra-low-power (ULP) Wake-up Receiver (WuRx); b) Circuital representation of a WuRx implementing a mechanical resonator as matching network (MN) in place of a commercial inductor. The MEMS resonator is modeled via Butterworth-Van Dyke (BVD) model [12]; and c) Simulated resonator admittance (solid blue) and simulated input admittance (dashed blue) of the MN when resonator is interfaced in series with a capacitor (C_{load}), showing characteristic resonance frequency pulling. On right axis, simulated passive voltage amplification (G_v) provided by the resonator to C_{load} (red).

In its inductive region, it enables resonant passive voltage gain across the load capacitor [13]. With standard phasor analysis it can be shown that maximum attainable gain is:

$$G_v = \left| \frac{Z_{load}}{R_{in} + R_{MN}} \right| \tag{1}$$

where Z_{load} represents the impedance of the output node, R_{in} the antenna's input impedance, and R_{MN} the resistance introduced by the matching network. For the reported configuration, R_{MN} can range between 2 and 4 times the motional resistance (R_m, Fig.1b) of the resonator [14]. The passive voltage amplification peak occurs at an offset frequency (f_{RF}), compared to the natural resonant frequency of the resonator (f_s), as in Fig.1c [14].

B. Gain from Y-parameters

The gain can, theoretically, be calculated from the measured resonator scattering parameters (S). An example of measurement setup to extract the S-parameters is reported in Fig. 2a. The two electrical nodes of the resonators are tested as the through nodes of a two-port network. The resonator admittance can be calculated as $-Y_{12}$, where Y is the admittance matrix derived from the measured S-parameters. In this case, the gain provided by the 2-port network when interfaced to an arbitrary source at port 1 and load at port 2 can be expressed as:

$$G_v = \left| \frac{V_2}{V_{in}} \right| \tag{2}$$

where V_{in} is the source voltage and V_2 the voltage at the output node (Fig.2b). By knowing that $V_1 = V_{in} - I_1 R_{in}$ and $I_2 = -j\omega C_{load} V_2$ (Fig.1b), it is possible to describe the system as follow:

$$\begin{bmatrix} I_1 \\ -V_2 j\omega C_{load} \end{bmatrix} = \begin{bmatrix} Y_{11} & Y_{12} \\ Y_{21} & Y_{22} \end{bmatrix} \begin{bmatrix} V_{in} - I_1 R_{in} \\ V_2 \end{bmatrix} \tag{3}$$

By solving the linear system, it is straightforward to extract V_2 and estimate G_v. It is worth noticing that this model takes into account all the signal-ground (Y_p) and feedthrough (Y_f) parasitics.

C. Gain from Y_{12}

If the parasitics to ground can be neglected (*e.g.*, if the chip is insulated from the ground), the sole Y_{12} (or Y_{21}) parameter can be used to estimate the gain. In this case, the gain can be expressed as:

$$G_v = \left| \frac{Z_{load}}{(R_{in} + \frac{1}{-Y_{12}} + Z_{load})} \right| \tag{4}$$

According to the model reported in Fig.2b, only the feedthrough parasitics might be affecting G_v simulated value. As reported in Fig.2c, these parasitics include real device feedthrough resistance (R_f) and capacitance (C_f), but also potential measurements artifacts (R_{pVNA} and C_{pVNA}).

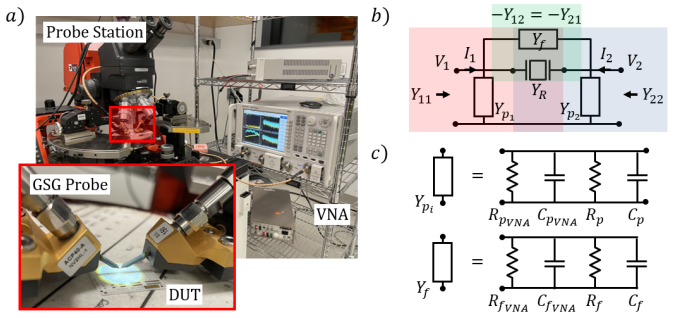

Fig. 2. a) Scattering (S) parameter measurement setup. A Keysight N5221A Vector Network Analzyer (VNA) is connected via coaxial cables to two Form Factor Cascade ACP GSG-150 probes. The GSG probes are landed on the desired Device Under Testing (DUT) for S-parameters extraction; b) Schematic representation of the admittance (Y) parameters of an electrical 1-port device measured in a 2-port configuration. For this π network, $Y_{ii} = Y_{p_i} + Y_R + Y_f$, while $Y_{ij} = -(Y_R + Y_f)$ [15]; and c) Modeling of the signal-to-ground (Y_{p_i}) and feedthrough (Y_f) parasitics.

D. Gain from Y_{fit}

Alternatively, G_v can be simulated by using fitted resonator data extracted from Y_{12} in place of the two-port measured resonator data. While this approach is theoretically identical to the one reported in the previous section, in practice, this can overcome the impact of Y_{p_i} and Y_f arising from two-port measurements. In this case, the admittance is approximated by means of a multi Butterworth-Van Dyke (mBVD) model such as $-Y_{12} \approx Y_{fit}$:

$$Y_{fit} = j\omega C_0 + \sum \frac{1}{R_{mi} + j\omega L_{mi} + \frac{1}{j\omega C_{mi}}} \tag{5}$$

Similarly to 4, G_v can be expressed as:

$$G_v = \left| \frac{Z_{load}}{(R_{in} + \frac{1}{Y_{fit}} + Z_{load})} \right| \tag{6}$$

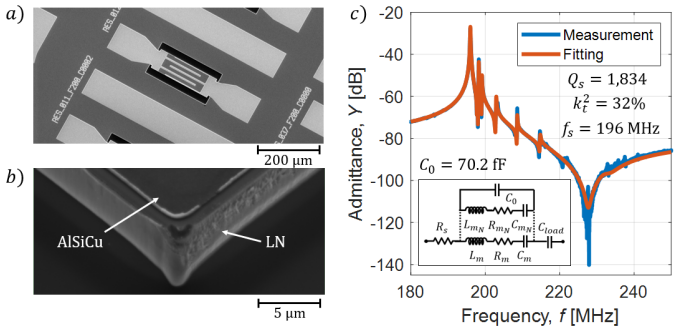

Fig. 3. a) SEM picture of a fabricated 30°XZ X-cut Lithium Niobate S_0 mode resonator operating around 200 MHz; b) Zoom-in of the edge of the resonator plate. The adopted fabrication process is reported in [8]; and c) Admittance (Y_{12}) response and multi-BVD fitting [16] (cfr. inset) of the resonator used to benchmark the different gain models. Spurious modes parameters: f_s = [198.272 199.121 208.598 212.255 197.821 202.95 232.540 237.501 221.948 214.75] MHz, Q_s = [2716 2464 1687 3.521 3764 1200 54 0.039 0.039 1000], and k_t^2 = [0.036 0.017 0.0023 0.0064 0.0046 0.010 0.001 0.002 0.0022 0.001].

III. Measurements and Discussion

A. Device Measurement and Parasitics Extraction

In this paper, a fabricated 30° YZ X-cut Lithium Niobate (LN) S_0 resonator is used as benchmark to evaluate the different gain models reported in Section II. An SEM image of the resonator is reported in Fig.3a-b, while the complete fabrication process and more details can be found in [8]. The electrical properties of the resonator are extracted by direct wafer probing in laboratory conditions using Form Factor Cascade ACP GSG-150 probes, while the S-parameters are recorded with a Keysight N5221A Vector Network Analyzer (VNA). The short-open-load-through (SOLT) calibration is performed on a ISS 101-190 calibration kit implementing an intermediate frequency (IF) bandwidth of 300 Hz.

To extract multi-modal mBVD model data, a dynamic fitting engine was developed in MATLAB® and is available as part of a collaborative project [16]. The resonator measurement and the relative mBVD fitting are reported in Fig.3c. An on-chip open structure including pads and resonator's routing is measured to extract the ground and through parasitics, as in Fig.2b-c. The open structure measurement are reported in Fig.4a-d.

While the susceptance of Y_{11} and Y_{12} allow to properly extract the capacitance values of the model (Fig.4a-c), the VNA noise floor does not allow the extraction of the resistances, which are extremely sensitive to calibration values and measurement setup (reflection or transmission). Both the real components of Y_{11} and Y_{12} show, in fact, the typical behavior of a delay line and values spanning several order of magnitude. Ultimately, both the real components of Y_{11} and Y_{12} assume unrealistic values in several regions of the investigated spectrum, rising concern on the use of measured one and two-port S-parameters for passive voltage gain estimation.

To cross-check the values and trends of pad parasitics, an electromagnetic (EM) simulation of the open structure is performed via ADS Momentum® engine. The stacking adopted for the EM simulation is reported in Fig.5 and reflects the device structure. The simulations results are reported in Fig.5c, showing values of C_p and C_f of 24 and 3 fF respectively, consistently with the VNA measurements. However, simulated R_p and R_f of 1 and 9 MΩ confirm that the measured values are limited by VNA resolutions, and must be therefore considered artifacts. The values extracted from the EM simulations are included in the Y_{fit} resonator modeling for consistence.

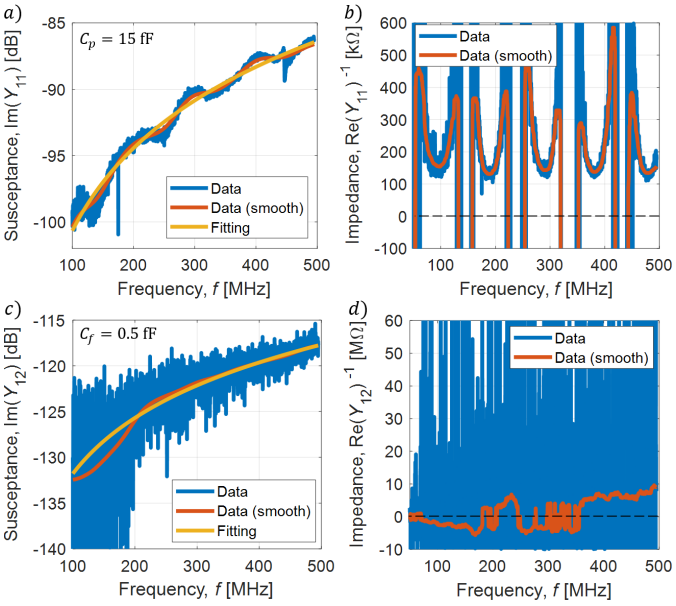

Fig. 4. On-chip test structure measurements: a) Extracted susceptance (measured from Y_{11}) and relative fitting to extract C_p+$C_{p_{VNA}}$ = 15 fF; b) Extracted resistance (measured from Y_{11}) $R_p||R_{p_{VNA}}$; c) Extracted susceptance (measured from Y_{12}) and relative fitting to extract $C_f + C_{f_{VNA}}$ = 0.5 fF; and d) Extracted resistance (measured from Y_{12}) $R_f||R_{f_{VNA}}$. Fitting is performed on the data smoothed with a gaussian filter. While it was possible to estimate C_p and C_f, resistance extraction was proven to be impossible with this technique, as both ground and feedthrough resistance include negative values, and thus they should be considered measurements artifacts.

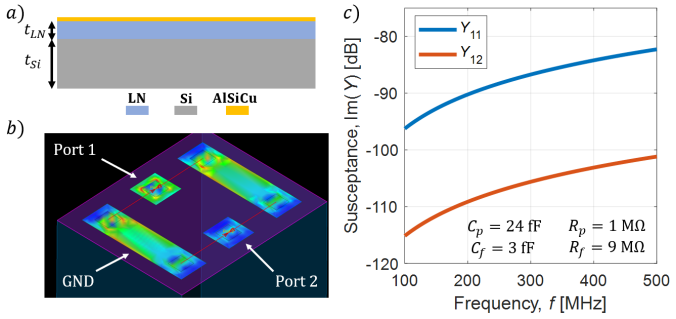

Fig. 5. Electromagnetic (EM) simulations performed with ADS Momentum®. a) EM simulation stack, composed of a top perfect conductor, a 1 µm thin film of $LiNbO_3$ (ε_r = 43 and $tan\delta$ = 40 ppm), and a 500 µm high-resistivity silicon substrate (ε_r = 9 and ρ = 20 kΩ cm); b) Simulated current density profile assuming excitation at Port 1; and c) Extracted susceptances from simulated data. C_p, C_f, R_p, and R_f are also reported.

B. Gain Comparison

To evaluate the accuracy of the proposed models including the above mentioned artifacts, G_v is simulated according to all the aforementioned methods. The simulations are then compared to the direct voltage amplification measurement performed with two GGB Industries Picoprobe (19C+34A) on the DUT with a know load of 270 fF, which provided

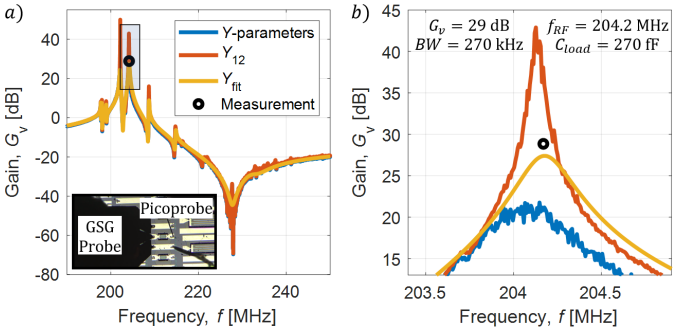

Fig. 6. a) Simulated G_v of the aforementioned models compared with measurements of the voltage provided by an actual device, according to the procedure reported in [8]. A picture of the DUT is reported in the inset; and b) Zoom-in of the peak region.

29 dB of gain at 203 MHz. The procedure for direct G_v extraction is reported in [8]. According to the results reported in Fig.6, the method implementing the resonator fitting (Y_{fit}) and the results from the EM simulation is the most accurate in forecasting G_v. On the other hand, the method based on the full Y-parameter matrix underestimates the gain by 10 dB due to the presence of the artifact low R_p to ground, while the Y_{12} method overestimates the gain by 10 dB due to the presence of an artifact negative value of R_f placed in parallel with the device.

IV. Conclusions

In this paper, different methods to simulate the gain provided by high-performance MEMS resonators in novel, Internet of Things receivers' matching networks are investigated. The results reported in this work highlight the limitations introduced by using direct measurements for gain simulations, due to the limited resolution of the commonly available test instruments when high-performance substrates are used. A method combining device fitting and electromagnetic simulation of the parasitic is proved to be the most accurate in simulating the gain provided by such systems.

References

[1] R. H. Olsson, R. B. Bogoslovov, and C. Gordon, "Event driven persistent sensing: Overcoming the energy and lifetime limitations in unattended wireless sensors," in *2016 IEEE SENSORS*, pp. 1–3, 2016.

[2] P. Bassirian, J. Moody, and S. M. Bowers, "Event-driven wakeup receivers: Applications and design challenges," *Midwest Symposium on Circuits and Systems*, vol. 2017-August, pp. 1324–1327, sep 2017.

[3] C. Gray, R. Ayre, K. Hinton, and R. S. Tucker, "Power consumption of IoT access network technologies," *2015 IEEE International Conference on Communication Workshop, ICCW 2015*, pp. 2818–2823, sep 2015.

[4] J. Moody, S. Gong, B. H. Calhoun, S. M. Bowers, A. Dissanayake, H. Bishop, R. Lu, N. Liu, D. Duvvuri, A. Gao, D. Truesdell, and N. S. Barker, "A Highly Reconfigurable Bit-Level Duty-Cycled TRF Receiver Achieving -106-dBm Sensitivity and 33-nW Average Power Consumption," *IEEE Solid-State Circuits Letters*, vol. 2, pp. 309–312, dec 2019.

[5] X. Shen, D. Duvvuri, P. Bassirian, H. L. Bishop, X. Liu, A. Dissanayake, Y. Zhang, T. N. Blalock, B. H. Calhoun, and S. M. Bowers, "A 184-nW, -78.3-dBm Sensitivity Antenna-Coupled Supply, Temperature, and Interference-Robust Wake-Up Receiver at 4.9 GHz," *IEEE Transactions on Microwave Theory and Techniques*, 2021.

[6] P. Bassirian, J. Moody, R. Lu, A. Gao, T. Manzaneque, A. Roy, N. Scott Barker, B. H. Calhoun, S. Gong, and S. M. Bowers, "Nanowatt-Level Wakeup Receiver Front Ends Using MEMS Resonators for Impedance Transformation," *IEEE Transactions on Microwave Theory and Techniques*, vol. 67, pp. 1615–1627, apr 2019.

[7] P. Bassirian, J. Moody, A. Gao, T. Manzaneque, B. H. Calhoun, N. S. Barker, S. Gong, and S. M. Bowers, "A passive 461 MHz AlN-CMOS RF front-end for event-driven wakeup receivers," in *2017 IEEE SENSORS*, pp. 1–3, 2017.

[8] L. Colombo, M. E. Galanko Klemash, T. M. Kiebala, S. S. Bedair, G. Piazza, and M. Rinaldi, "VHF and UHF Lithium Niobate MEMS Resonators Exceeding 30 dB of Passive Gain," *IEEE Electron Device Letters*, vol. 42, pp. 1853–1856, Dec 2021.

[9] R. Lu and S. Gong, "RF acoustic microsystems based on suspended lithium niobate thin films: advances and outlook," *Journal of Micromechanics and Microengineering*, vol. 31, p. 114001, sep 2021.

[10] S. Gong, R. Lu, Y. Yang, L. Gao, and A. E. Hassanien, "Microwave Acoustic Devices: Recent Advances and Outlook," *IEEE Journal of Microwaves*, vol. 1, pp. 601–609, apr 2021.

[11] X. Zhao, B. Herrera, and C. Cassella, "Record-High K T2 Exceeding 7.4% Through Low-Impedance Lithographically Defined Resonant Rods in Aluminum Nitride Thin Plates," *Proceedings of the IEEE International Conference on Micro Electro Mechanical Systems (MEMS)*, vol. 2020-January, pp. 1278–1280, jan 2020.

[12] G. Piazza and H. Bhugra, eds., *Piezoelectric MEMS Resonators*. Microsystems and Nanosystems, Springer International Publishing, 2017.

[13] L. Colombo, A. Kochhar, G. Vidal-Álvarez, and G. Piazza, "High-Figure-of-Merit X-Cut Lithium Niobate MEMS Resonators Operating Around 50 MHz for Large Passive Voltage Amplification in Radio Frequency Applications," *IEEE Transactions on Ultrasonics, Ferroelectrics, and Frequency Control*, vol. 67, no. 7, pp. 1392–1402, 2020.

[14] L. Colombo, A. Kochhar, G. Vidal-Alvarez, and G. Piazza, "High Figure of Merit X-cut Lithium Niobate MEMS Resonators Operating Around 50 MHz for Large Passive Voltage Amplification in Radio Frequency Applications," *IEEE Transactions on Ultrasonics, Ferroelectrics, and Frequency Control*, p. 1, feb 2020.

[15] D. M. Pozar, *Microwave Engineering; 3rd ed.* Hoboken, NJ: Wiley, 2005.

[16] G. Michetti, "PiezoResFitting." https://github.com/giumc/PiezoResFitting, 2020. [Online].